CILAMCE 2017
Florianópolis - Santa Catarina - Brazil

A SIMPLIFIED NON-LINEAR POROELASTIC APPROACH TO TRANSIENT EFFECTS INDUCED BY CYLINDER ROTATION IN A POROUS MEDIUM

Gracieli Dienstmann

g.dienstmann@gmail.com

Adrien Fayolle

Felipe S. de Almeida

Fernando Schnaid

Samir Maghous

fayolle.adrien@gmail.com

schaedleralmeida@gmail.com

fschnaid@gmail.com

samir.maghous@ufrgs.br

Department of Civil Engineering, Federal University of Rio Grande do Sul

Avenida Osvaldo Aranha, 99 - Centro Histórico, 90035-190, Porto Alegre, Brasil

Abstract. *Drainage conditions associated with loading rate effects during in situ vane-like tests are fundamental factors in the assessment and interpretation of shear strength properties of intermediate permeability soils. In that context, a simplified model for poromechanical analysis of consolidation induced by rotation of a rigid cylinder embedded within a porous medium is formulated. The approach is closely connected with the concept of deformation plasticity and relies upon the equivalence between the local behavior of a poroplastic material under monotonic loading process and that of an appropriate non-linear fictitious poroelastic behavior. The non-linear poroelastic model is conceived to capture the transient flow effects on the poromechanical response of the soil surrounding the rotating cylinder. Semi-analytical solutions are derived for pore-fluid pressure, displacement and stress distributions, allowing for the evaluation of rate effects in silty soils, with specific application to frictional-cohesive materials. The accuracy of the approach is assessed by comparison of model predictions with poroplastic finite element solutions. The results correlating the degree of drainage to normalized rotation velocity derived from proposed model may be a useful support for interpretation of in situ measured properties and foundation design purposes.*

Keywords: *Non-linear poroelasticity, Transient flow, rotating cylinder, Finite element analysis.*

1 INDRODUCTION

The theory of poroelasticity is a well-established engineering framework for studying the fluid flow process through porous materials where the solid matrix is elastic, allowing stresses, displacements and pore fluid pressure to be calculated under different loading conditions. The theory developed by Biot (1941) and contextualized by de Boer (2000); Wang (2000), Coussy (2004), Selvadurai (2007) and others considers the solid matrix and the fluid as a homogeneous continuum where the flow and the pressure gradient are linked by a Darcy type relation using a permeability coefficient.

In the present paper, the Biot consolidation analysis is applied to the problem of an infinite long solid cylinder rotating in a porous isotropic elastic medium. Since the drainage condition in saturated soils generally depend on permeability, compressibility, shear strength and loading rate (Silva et al, 2005; Lehane et al, 2009; Kim et al, 2008; Schneider et al, 2007), a change in the rate of loading is expected to produce variations in the pore-fluid pressure profile, thus inducing changes in the strength and stiffness of the soil. In that respect, a key issue in geotechnical engineering is the possibility to evaluate the variations in the strength and stiffness of the soil and to assess the way they influence the design of problems such as piles, shafts, tunnels or *in situ* test.

In the absence of published solutions or testing data that could be used as reference, the theoretical modeling developed in this paper seeks primarily to provide a simplified poromechanics-based tool for predicting pore pressure rate effects induced by rotation of a rigid cylinder within a porous medium. In particular, the analysis is able to identify the drainage conditions taking place around elements rotating at different loading rates. Evaluation of these drained effects is based on the normalization of rotation tests characterized by an analytical drainage characterization curve represented in the degree of drainage versus a non-dimensional parameter space (e.g. Randolph and Hope, 2004), where:

$$\overline{V} = \frac{V\ d}{c_h} \tag{1}$$

where d is the probe diameter, V the loading rate and c_h the coefficient of consolidation. This framework has been extensively used recently to determining experimentally rate effects taking place during penetration and rotation of *in situ* tests (House et al, 2001; Schnaid et al, 2004; Randolph & Hope, 2004; Chung et al, 2006; Schneider et al, 2007; DeJong, 2012). Yet few attempts have been made to develop a structured theoretical frame to anticipate drained conditions in intermediate permeability soils (Silva et al, 2005; Ref.), which is the aim of the present research.

2 PROBLEM STATEMENT AND FRAMEWORK OF ANALYSIS

This section describes the main features of the simplified poromechanics model adopted for the analysis of consolidation induced by rotation of a rigid cylinder deeply embedded within an isotropic elastic medium of infinite extent. The cylinder is subjected to a prescribed rotation-like displacement and its geometry may be viewed as a simple conceptual model of a pile, shield, shaft or vane test, and the associated solution would then be relevant to the consolidation of soil around the cylinder induced by its rotation during related *in situ* shear.

Proceedings of the XXXVIII Iberian Latin-American Congress on Computational Methods in Engineering
P.O. Faria, R.H. Lopez, L.F.F. Miguel, W.J.S. Gomes, M. Noronha (Editores), ABMEC, Florianópolis, SC, Brazil, November 5-8, 2017.

The analysis presented in the sequel is based on the assumption of plane strain conditions in the cross-section of a system defined by the cylinder and surrounding porous medium, restricting displacements and flow to two-dimensions setting (Fig. 1).

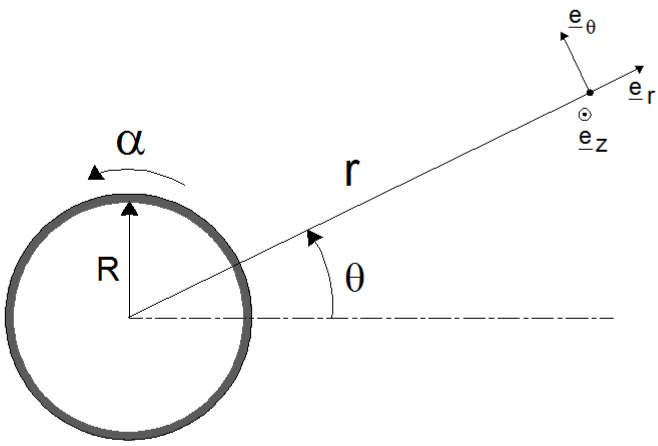

Figure 1. Geometry model for consolidation around infinite rotating cylinder.

The soil surrounding the rotating cylinder is modeled as a fully saturated poroelastic material undergoing infinitesimal strains. At the macroscopic scale, the representative elementary volume is the superposition of both solid and fluid particles that are located at the same geometrical point (Coussy, 2004; Dormieux et. al, 2006). The skeleton is the macroscopic perception of the solid phase.

2.1 Governing equations for stress and displacement fields

In all what follows, the sign convention of positive stress values for tension and negative stress values for compression will be adopted. Denoting $\underline{\underline{\sigma}}_0$ and p_0 the initial fields of stress and pore-fluid pressure in the medium, the poroelastic state equations for an isotropic material can be expressed within the framework of infinitesimal strains as

$$\Delta\underline{\underline{\sigma}} = \lambda \operatorname{tr}\underline{\underline{\varepsilon}}\,\underline{\underline{1}} + 2G\underline{\underline{\varepsilon}} - b\Delta p\underline{\underline{1}} \tag{2}$$

$$\Delta\phi = b \operatorname{tr}\underline{\underline{\varepsilon}} + \frac{1}{M}\Delta p \tag{3}$$

where λ and G are the Lamé constants, b and M are respectively the Biot coefficient and Biot modulus. The first poroelastic state equation relates the stress change $\Delta\underline{\underline{\sigma}} = \underline{\underline{\sigma}} - \underline{\underline{\sigma}}_0$ to the skeleton infinitesimal strain $\underline{\underline{\varepsilon}}$ and pore-fluid pressure change $\Delta p = p - p_0$, while the second state equation relates the Lagrangian porosity change $\Delta\phi = \phi - \phi_0$ to the skeleton volumetric strain and fluid pressure change.

The *in-situ* stress, strain and fluid pressure fields induced by the insertion of the rigid cylinder and its subsequent rotation are in general significantly controlled by the non-linear behavior of the material. An approximate framework to capture some of these non-linear features consists in considering that the secant shear modulus G is evolving with the level of local shear strain and pore-fluid pressure induced by cylinder rotation. More precisely, we shall consider that the secant shear modulus depends on pore pressure p as well as on volumetric strain $\varepsilon_v = \mathrm{tr}\underline{\underline{\varepsilon}}$ and equivalent deviatoric strain $\varepsilon_d = \sqrt{(\underline{\underline{\varepsilon}} - \frac{1}{3}\mathrm{tr}\underline{\underline{\varepsilon}}) : (\underline{\underline{\varepsilon}} - \frac{1}{3}\mathrm{tr}\underline{\underline{\varepsilon}})}$. The idea consists basically in assuming that the local response of a plastic behavior under monotonic loading process can be conveniently simulated by means of a fictitious non-linear elastic behavior.

The starting point is the yield function characterizing the plasticity of the porous medium. In the present analysis, it is assumed that plasticity of the soil can be described by the following Drucker-Prager yield condition

$$F(\underline{\underline{\sigma}}') = \sigma_d + T\,(\sigma_m' - h) \leq 0 \tag{4}$$

where $\underline{\underline{\sigma}}' = \underline{\underline{\sigma}} + p\,\underline{\underline{1}}$ is the Terzaghi effective stress, $\sigma_d = \sqrt{(\underline{\underline{\sigma}} - \frac{1}{3}\mathrm{tr}\underline{\underline{\sigma}}) : (\underline{\underline{\sigma}} - \frac{1}{3}\mathrm{tr}\underline{\underline{\sigma}})}$ is the equivalent deviatoric stress and $\sigma_m' = \frac{1}{3}\mathrm{tr}\underline{\underline{\sigma}}' = \sigma_m + p$ is the mean Terzaghi effective stress. Material parameters h and T respectively refer to the tensile strength and the friction coefficient. The fictitious non-linear poroelastic material is then defined by imposing that the stress $\underline{\underline{\sigma}}$ associated with secant poroelastic behavior (2) meets asymptotically the above yield condition (4).

$$\lim_{\varepsilon_d/\varepsilon_{ref} \to \infty} F(\underline{\underline{\sigma}}' = \underline{\underline{\sigma}} + p\,\underline{\underline{1}}) = 0 \tag{5}$$

where ε_{ref} is a reference strain whose order of magnitude may evaluated from the elastic limit shear strain.

Following a reasoning similar to that developed in Lemarchand et al. (2002) and Maghous et al. (2009), the simplest choice for achieving condition (5) would consist in considering a constant value for the bulk modulus $K = \lambda + 2G/3$. In such a situation, and assuming an isotropic initial stress distribution (i.e., $\underline{\underline{\sigma}}_0 = \sigma_0\,\underline{\underline{1}}$), it is established that the asymptotic behavior for shear modulus reads

$$G(\varepsilon_d, \varepsilon_v, p) \approx \frac{T}{2\varepsilon_d}(h - K\varepsilon_v - \delta) \qquad \text{when } \varepsilon_d/\varepsilon_{ref} \geq 1 \tag{6}$$

Parameter δ is related to mean initial effective stress $\sigma_{0m}' = \frac{1}{3}\mathrm{tr}\underline{\underline{\sigma}}_0' = \sigma_{0m} + p_0$ and pore-fluid pressure through

$$\delta = \sigma'_{0m} + (1-b)\,\Delta p \tag{7}$$

Seeking to comply with the above condition (6), the approach proposed in Maghous et al. (2009) is extended to the context of poropelasticity by adopting the following dependence law for the secant shear modulus

$$G(\varepsilon_d, \varepsilon_v, p) = \frac{T}{2}(h - K\varepsilon_v - \delta) \times \frac{1/\varepsilon_{ref}}{1 + \varepsilon_d/\varepsilon_{ref}} \tag{8}$$

Figure 2 provides a non-linear poroelastic representation of the Drucker-Prager behavior as defined by equations (8).

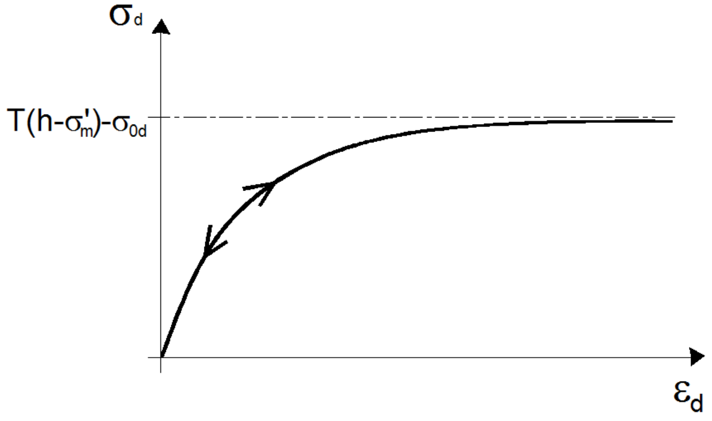

Figure 1. Representation of the non-linear elastic behavior associated with a Drucket-Prager yield condition.

The fictitious poroelastic behavior thus formulated involves a secant shear modulus that depends on the skeleton strain $(\varepsilon_d, \varepsilon_v)$ and pore-fluid pressure p. However, it should be pointed out that such a shear modulus is referring to a fictitious constitutive parameter, and not to a material property. Expression (8) stems from a mathematical equivalence between elastoplastic behavior and related non-linear elastic response and not from physical considerations.

Coming back to the initial problem of rotation of rigid cylinder embedded within a porous medium and related governing equations, the momentum balance equation satisfied by the stress field is first written:

$$\operatorname{div} \Delta \underline{\underline{\sigma}} = 0 \tag{9}$$

The above equilibrium equation should be completed by the mechanical boundary conditions related to the displacement $\underline{\xi}$:

$$\begin{cases} \underline{\xi} = \alpha\, R\, \underline{e}_\theta & \text{at } r = R \\ \underline{\xi} = 0 & \text{at } r = a > R \end{cases} \qquad \forall\, t > 0 \tag{10}$$

The first condition in (10) implies that a rotation angle α is imposed at the cylinder wall, while the second condition indicates that the displacement induced by the movement of the rigid cylinder is null at distance $a > R$. The latter parameter characterizes the extension of the zone of influence, that is, the distance beyond which the poromechanical state of the medium is no more affected by cylinder rotation. The concept of radius of influence has been introduced originally by Blight (1968) to model the *in situ* vane test, and has been extended to a wide range of consolidation problems. Based on experimental data or computational simulations, estimates for the relative size a / R of the zone of influence have been reported in the literature (e.g., by Blight, 1968; Vesic, 1972; Randolph and Wroth, 1979, Poulos and Davis, 1980, Morris and Williams, 2000; Osman and Randolph, 2010; Osman, 2010). These investigations indicate that ratio a / R depends on the soil Rigidity Index and ranges typically from $a / R = 5$ to $a / R = 60$.

Owing to problem symmetry, the displacement field within the porous medium is sought in the following form:

$$\underline{\xi} = f(r)\ \underline{e}_\theta + g(r)\ \underline{e}_r \tag{11}$$

For the sake of simplicity, the dependence of displacement functions f and g with respect to time shall be omitted in the sequel. The corresponding strain tensor reads

$$\underline{\underline{\varepsilon}} = \varepsilon_{rr}\ \underline{e}_r \otimes \underline{e}_r + \varepsilon_{\theta\theta}\ \underline{e}_\theta \otimes \underline{e}_\theta + \varepsilon_{r\theta}\,(\underline{e}_r \otimes \underline{e}_\theta + \underline{e}_\theta \otimes \underline{e}_r) \tag{12}$$

with

$$\varepsilon_{rr} = g'(r) \quad , \quad \varepsilon_{\theta\theta} = g(r)/r \quad , \quad \varepsilon_{r\theta} = \frac{1}{2}\left(f'(r) - f(r)/r \right) \tag{13}$$

and the non-zero components of stress increment associated with poroelastic law are

$$\begin{cases} \Delta\sigma_{rr} = \left[k - 2G/3\right]\left(g'(r) + g(r)/r\right) + 2G\, g'(r) - b\,\Delta p \\ \Delta\sigma_{\theta\theta} = \left[k - 2G/3\right]\left(g'(r) + g(r)/r\right) + 2G\, g(r)/r - b\,\Delta p \\ \Delta\sigma_{r\theta} = G\left(f'(r) - f(r)/r\right) \\ \Delta\sigma_{zz} = \left[k - 2G/3\right]\left(g'(r) + g(r)/r\right) - b\,\Delta p \end{cases} \tag{14}$$

which introduced into the local equilibrium equation (9) yield two differential equations governing the displacement functions $\left(f, g\right)$ and pore-fluid pressure p

$$\frac{\partial}{\partial r}\left[K\left(g'(r) + g(r)/r\right) + \frac{2G}{3}\left(2g'(r) - g(r)/r\right) - b\,\Delta p\right] + \frac{2G}{r}\left(g'(r) - g(r)/r\right) = 0 \tag{15}$$

and

$$\frac{\partial}{\partial r}\left[G\ \left(f'(r) - f(r)/r\right)\right] + 2G\,\frac{f'(r) - f(r)/r}{r} = 0 \tag{16}$$

It should be kept in mind that the above two differential equations are highly non-linear coupled through the shear modulus $G = G(\varepsilon_d, \varepsilon_v, p) = G\,(f, g, p)$, which is accordingly a function of the polar coordinate r (and also of time). The third differential equation for consolidation around the rotating cylinder is deduced from the solution to the fluid flow problem.

2.2 The fluid flow problem

The excess of pore pressure distribution generated by rotating a rigid cylinder stems from the solution of a hydraulic boundary value problem defined on the surrounding porous medium.

Neglecting the variations of fluid density ρ_f, the fluid mass balance writes in the context of infinitesimal skeleton strains

$$\frac{\partial\phi}{\partial t}+\operatorname{div}\underline{q}=0 \tag{17}$$

where $\underline{q}$ is the filtration vector. The latter is connected to the excess pore-fluid pressure u through the Darcy´s law

$$\underline{q}=-\underline{\underline{k}}\cdot\nabla u \tag{18}$$

$\underline{\underline{k}}$ denoting the permeability tensor.

In the subsequent analysis, the hydraulic properties for the porous medium are assumed to be isotropic: $\underline{\underline{k}}=k\,\underline{\underline{1}}$. Reporting both the second poroelastic state equation (3) expressed in rate form and the Darcy's law (18) into the fluid mass balance (17) yields

$$b\frac{\partial\,\mathrm{tr}\underline{\underline{\varepsilon}}}{\partial t}+\frac{1}{M}\frac{\partial\Delta p}{\partial t}=k\nabla^2 u \tag{19}$$

where ∇^2 stands for the Laplacian operator.

Extending a reasoning classically implemented in the context of linear poroelasticity (see for instance Coussy, 2004), the following equation can be derived from combining the non-linear pororoelastic constitutive equation (2) and the equilibrium equation (9)

$$\left(K+\tfrac{4}{3}G\right)\nabla\mathrm{tr}\underline{\underline{\varepsilon}}-G\,\mathrm{rot}\left(\mathrm{rot}\,\underline{\xi}\right)+2\,\nabla G\cdot\,(\underline{\underline{\varepsilon}}-\tfrac{1}{3}\mathrm{tr}\underline{\underline{\varepsilon}})=b\nabla\left(\Delta p\right) \tag{20}$$

The above identity (20) can be viewed as a generalized form for the Navier equation. It differs from the usual version by the term involving the spatial gradient of shear modulus.

On the other hand, it can be readily shown that the projection of equation (20) following the ortho-radial direction reduces to the equilibrium equation (16), while its projection following the radial direction reads

$$\left(K+\tfrac{4}{3}G\right)\frac{\partial\,\mathrm{tr}\underline{\underline{\varepsilon}}}{\partial r}+\frac{2}{3}\frac{\partial G}{\partial r}\,\left(2g'(r)-g(r)/r\right)=b\frac{\partial\,\Delta p}{\partial r} \tag{21}$$

which emphasizes once again the strong coupling between skeleton strains and pore-fluid pressure. Unlike the usual formulations developed in linear poroelasticity, the pore-fluid pressure distribution is affected by the volumetric part $\varepsilon_v=\mathrm{tr}\underline{\underline{\varepsilon}}$ of skeleton strain as well as by the deviatoric part ε_d. This specific feature is a consequence of the shear modulus dependence with respect to $\underline{\underline{\varepsilon}}$ (see Eq. (8)).

From a theoretical viewpoint, the evaluation of the pore-fluid pressure p and displacement functions $\left(f,g\right)$ requires solving the coupled non-linear system defined by the set of three differential equations (15), (16) and (21). A comprehensive approach would therefore involve either sophisticated mathematics or numerical procedures, which fall beyond the scope of the present paper. Instead, a simplified time-incremental similar to that developed and described in Dienstmann et al (2017) will be used to handle this problem. The key idea consists of reformulating equation (21) by introducing an average shear modulus to approximate the non-linear shear modulus along each time interval.

Assuming that an equivalent mean shear modulus $G \approx G_{eq}$, constant with respect to time variable and space coordinates, can be evaluated for each time interval $t_n \le t \le t_{n+1}$. In that case, equation (21) is integrated with respect to radial coordinate

$$\left(K+\tfrac{4}{3}G_{eq}\right)\,\mathrm{tr}\underline{\underline{\varepsilon}} = b\,\Delta p + C(t) \tag{22}$$

Keeping in mind that the poromechanical state of the medium is not affected by installation and rotation of the rigid cylinder beyond the zone of influence (i.e., $\underline{\underline{\varepsilon}}(r,t) = \Delta p(r,t) = 0$ for $r > a$), it turns out that integration $C(t)$ function is null. A classical reasoning that relies upon equations (19) and (22), together with equality $\frac{\partial \Delta p}{\partial t} = \frac{\partial u}{\partial t}$, allows to obtain an uncoupled pore-fluid pressure diffusion equation

$$\frac{\partial u}{\partial t} = c_f\ \nabla^2 u \qquad \text{with} \qquad c_f = k\,M\,\frac{\left(K+\tfrac{4}{3}G_{eq}\right)}{Mb^2+\left(K+\tfrac{4}{3}G_{eq}\right)} \tag{23}$$

Parameter c_f represents the equivalent fluid diffusivity coefficient for time interval $[t_n\,,t_{n+1}]$. The above equation is analogous to that derived in Randolph and Wroth (1979) or Coussy (2004), the difference being only in the expression form of diffusivity coefficient.

A simplest way to define an equivalent shear modulus consists therefore in considering for each time interval $[t_n\,,t_{n+1}]$ the spatial average

$$G_{eq}(t_n) = \frac{1}{a-R}\int_R^a G\left(\varepsilon_d(r,t_n)\,;\,\varepsilon_v(r,t_n)\,;\,p(r,t_n)\right)dr \tag{24}$$

It should be emphasized that the concept of equivalent shear modulus $G \approx G_{eq}$ along time interval $[t_n\,,t_{n+1}]$, is only introduced for the pressure diffusion equation, whereas the non-linear expression of shear modulus will be preserved in equilibrium equations (15) and (16).

2.3 Incremental-iterative procedure for the poroelastic problem

The uncoupled flow problem along time interval $t_n \le t \le t_{n+1}$ is defined by the diffusion equation (23), together with the hydraulic boundary and initial conditions:

$$\begin{cases} \partial u/\partial r = 0 & \text{at } r = R\ ;\ \forall\, t\in[t_n,t_{n+1}] \\ u = 0 & \text{at } r = a\ ;\ \forall\, t\in[t_n,t_{n+1}] \\ u = u(r,t_n) & \text{at } t = t_n\ ;\ \mathrm{R} \le r \le a \end{cases} \tag{25}$$

The first equation in (25) is the impermeability condition at the rigid cylinder wall, while the second equation expresses that the excess pore pressure induced by rotation of the rigid cylinder is fully dissipated at the radius of influence, and the third equation refers to the initial pore fluid pressure at time $t = t_n$.

Starting the test modeling at $t=0$, the initial pore pressure will be referred to as $u_0(r)=u(r,t=0)$. The dependence of the latter with respect to radial coordinate is intended to account for the excess pore pressure that is induced by installation of the rigid cylinder in the soil mass. Evaluation of the initial excess pore pressure distribution is generally based on laboratory and *in situ* investigations. This fundamental component of the modeling will be discussed in the next section.

The general solution to the boundary value problem defined by equations (23)-(25) reads

$$u(r,t)=\sum_{i=1}^{\infty} C_i^* \left[\omega_i Y_0(\alpha_i r)-J_0(\alpha_i r)\right] e^{-c_f \alpha_i^2 (t-t_n)} \tag{26}$$

where

$$C_i^* = \frac{\int_R^a u\ (r,t_n)\ [\varpi_i Y_0(\alpha r)-J_0(\alpha r)]\, r\, dr}{\int_R^a [\varpi_i Y_0(\alpha r)-J_0(\alpha r)]^2\ r\, dr} \tag{27}$$

Functions J_0 and Y_0 are zero-order Bessel functions of the first and second kind respectively. The scalar α_i is the i-th root of the following algebraic equation with respect to variable x

$$Y_1(xR)\ J_0(xa)-J_1(xR)\ Y_0(xa)=0 \tag{28}$$

where J_1 and Y_1 are first-order Bessel functions referring respectively to the first and second kind. The scalar ω_i is computed from α_i as

$$\omega_i=-Y_1(\alpha_i R)/J_1(\alpha_i R) \tag{29}$$

Once the excess pore-fluid pressure u is computed from equations (26) to (29), the pore-fluid pressure increment can thus be determined as $\Delta p=u-u_0$.The latter is therefore substituted into equations (15) and (16) that govern the displacement $\underline{\xi}=f(r,t)\ \underline{e}_\theta+g(r,t)\ \underline{e}_r$ of skeleton particles during time interval $t_n \le t \le t_{n+1}$. For each time t within this interval, the system formed by the differential equations (15) and (16), together with associated boundary conditions:

$$\begin{cases} f(R,t)=\alpha R \quad ; \quad g(R,t)=0 \\ f(a,t)=0 \quad ; \quad g(a,t)=0 \end{cases} \qquad \forall\ t>0 \tag{30}$$

is solved iteratively with implementation of a specific numerical procedure. At each iterative step, integration of differential equations (15) and (16) is achieved by a finite difference scheme.

The iterative algorithm used for the evaluation of pore-fluid pressure distribution and displacement functions during time step $\Delta t=t_{n+1}-t_n$ can be assessed in Fayolle (2016).

2.4 Initial excess pore pressure distribution

A fundamental input of the model is the value of initial excess pore-fluid pressure that prevails in the porous medium prior to cylinder rotation. Indeed, the simplified framework formulated in the preceding section that allows derive analytically the pore-fluid pressure $u(r,t)$ (see equations (26) to (29)), requires the initial pore pressures distribution to be known. In this regard, the following alternative distribution which was discussed in Dienstmann et. al (2017) will be suggested:

$$u_0(r) = u_{0,\max}\frac{\mathfrak{F}(r)}{\mathfrak{F}(R)} \quad with\ \mathfrak{F}(r) = 1 - \frac{a_0}{r} + \frac{a_0}{R}\ln\frac{a_0}{r} \qquad \text{for} \quad R \le r \le a_0 \tag{31}$$

A main feature of all above expressions formulated for initial excess pore-fluid pressure $u_0(r)$ is their dependence on $u_{0,\max} = u(r = R)$, which represents the maximum excess pore pressure generated by the installation process. Correlating the pile insertion into the soil with a cavity expansion problem, typical solutions derived in this context (e.g. Vésic 1972; Randolph and Wroth 1979) suggest that $u_{0,\max}$ can be evaluated from the stress paths developed in undrained triaxial tests carried out until the ultimate state (undrained strength) is attained. The excess pore-fluid pressure is thus deduced from the variation in mean and shear stresses, leading to the following estimate for normally consolidated soils:

$$u_{0,\max} = \frac{p_{c0}}{2}\left(1 + M_{cs}\right) \tag{32}$$

Parameter p_{c0} is a reference initial consolidation pressure, and M_{cs} refers to the slope of the critical state line. It should be emphasized that expression (32) implicitly assumes that cylinder installation is fast, the elapsed time between installation and rotation is sufficiently short for pore-fluid pressures do not dissipate, thus justifying the assumption of undrained hydromechanical evolution of soil.

Expression (30) of initial excess pore-fluid pressure $u_0(r)$ will be used as a reference in the numerical simulations provided in section 3, together with values for the extension of the zone of influence that are as high as $a = 100\,R$, which fall within the range proposed in previous investigations as discussed earlier in the paper.

3 NUMERICAL ANALYSIS

The simplified model developed for consolidation around a rotating cylinder has been formulated within the framework of non-linear poroelasticity, extending the concept of deformation (or Henky) plasticity to porous media. The semi-analytical solution for pore-fluid pressure, stress and displacement fields induced by cylinder rotation, relies upon the implementation of an incremental-iterative algorithm and numerical evaluation of functions (f, g). As previously mentioned, the latter evaluation is achieved by resorting to a finite difference scheme. The model predictions are compared to fully coupled poroplastic finite element solutions using the standard ABAQUS software. The aim of this comparison is to assess the ability of the non-linear poroelastic modeling to macroscopically capture essential features of deformation induced by cylinder rotation in the poroplastic porous medium. The effects of drainage into the porous medium, notably drainage conditions in a silty soil (transient materials), will be specifically investigated.

In the subsequent numerical illustrations, the value of hydrostatic fluid pressure along the plane of analysis is adopted as reference value for pore pressures in the porous medium.

A series of numerical simulations have been performed considering the following set of data:

$$\begin{aligned} &K = 20\ \text{MPa}\ ;\ \varepsilon_{ref} = 10^{-3}\ ;\ b = 0.98\ ;\ M = 2.3\ \text{GPa}\ ;\ c = 2\ \text{kPa}\ ;\ \phi = 25^{\circ}\ ; \\ &k = 10^{-8}\ \text{m/s}\ ;\ \sigma_0 = -150\ \text{kPa}\ ;\ u_{0,\max} = 100\ \text{kPa}\ ;\ a_0 \in \{10R\ ,\ 25R\}\ ;\ a = 100R \end{aligned} \tag{33}$$

a cohesive-frictional porous medium which is described by a Drucker-Prager constitutive model associated with the effective stress yield condition (4). Drucker-Prager strength parameters h and T are computed from cohesion c and friction angle ϕ that define the inscribed Mohr Coulomb yield surface ($h = c/\tan\phi$ and $h = 6\sin\phi/(3-\sin\phi)$). The initial poromechanics state is defined by an isotropic stress field $\underline{\underline{\sigma}}_0 = \sigma_0 \underline{\underline{1}}$ and the pore-fluid pressure distribution (30). The loading process in the analyzed problem consists in increasing the prescribed displacement $\xi_\theta = \alpha R$ imposed at the rigid cylinder wall, from zero to a maximum value corresponding to the end of the "rotation test". For comparison purposes, the latter is defined in all simulations by fixing arbitrarily the maximum value of shear strain at cylinder wall to $\varepsilon_d = 10\%$, which could be considered from a practical geotechnical engineering viewpoint as a limit for the validity of infinitesimal strains analysis. However, it should be kept in mind that a more theoretical approach would require the problem to be handled within the framework of large strains.

Referring to the characteristic velocity $V_c = c_f / R$ associated with poroelastic consolidation phenomenon, three typical values for rotation rate $V = \dot{\alpha} R$ are investigated in the analysis. They range from $V = 10^{-5}$ mm/s which is characteristic of drained evolution of the porous medium during the test, to $V = 10^{-3}$ mm/s for partially drained evolution, and $V = 1$ mm/s that is considered to be representative of undrained response of the soil surrounding the rotating cylinder.

Aiming to assess the accuracy of the modeling, the non-linear poroelastic predictions derived in the context of frictional-cohesive soil are compared to finite solutions obtained in the framework of plastic constitutive modeling using ABAQUS software. The consolidation problem induced by cylinder rotation is handled as a plane strain problem in the plane normal to the vertical direction. The discretized soil domain used in the finite element simulations is sketched in Figure 4, together with appropriate poromechanical boundary conditions. The extension of the geometry domain is fixed to $a = 100R$, which proves sufficient to simulate remote boundary conditions. The finite element mesh is composed of 8-node quadrilateral elements (CAX8RP), corresponding to piecewise quadratic approximation for skeleton displacement and piecewise linear approximation for pore-fluid pressure. Size and dimensions and the finite element discretization have been selected from preliminary mesh sensitivity (convergence) analysis considering different spatial geometry discretization. The mesh selected for subsequent simulations consisted of 52000 quadrilateral elements and total number of nodes equal to 156800, corresponding to 366000 total degrees of freedom: 313600 for displacement and 52400 for pore-fluid pressure. The aspect ratio of elements (ℓ_θ / ℓ_r) varies from 2 at the cylinder wall ($r = R$) to 0.25 for elements located at $r = a$. It is pointed out that the poroplastic model adopted in the finite element simulations assumes linear poroelastic properties as well as perfect plasticity. The associated values of material parameters are the same as those defined in (33), except for the elastic shear modulus which is taken equal to $G_0 = G(\varepsilon_d = 0, \varepsilon_v = 0) = T(h - \sigma'_{0m})/2$. In addition, the dilatancy angle required for definition of the poroplastic model that has been fixed to $\psi = 0^\circ$.

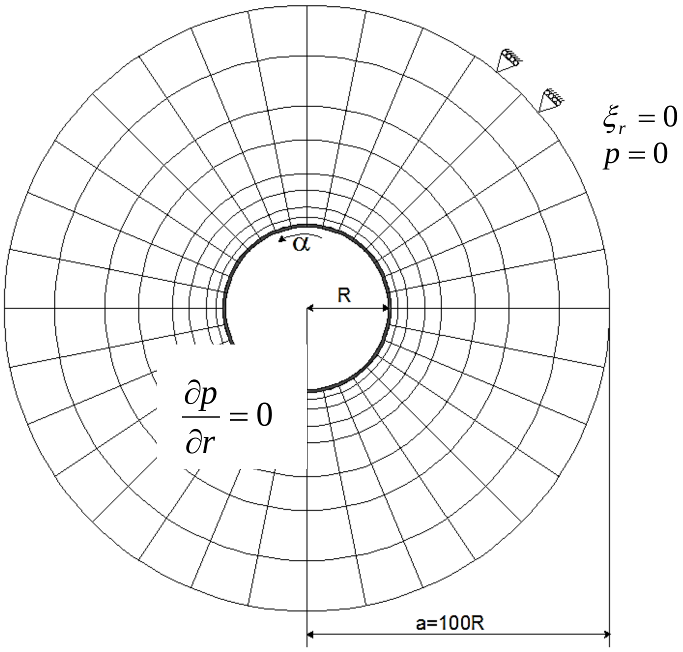

Figure 4: Schematized finite element discretiozation (not at scale) and associated boundary conditions

An important interpretation aspect is the soil behavior at the rotating cylinder wall, since the value of applied torque associated with the prescribed displacement at $r = R$ is directly controlled by the stress distribution along the cylinder circumferential area. This behavior is firstly illustrated by plotting the variations of shear stress $q_u = \sigma_d(r = R)$, normalized by the material strength parameter $T \times h$, mobilized at the cylinder wall as a function of equivalent deviatoric strain ε_d (Fig. 12). It is first emphasized that numerical difficulties raised when dealing with frictional materials by means of poroplastic F.E simulations. In both drained ($V = 10^{-5}$ mm/s) and partially drained ($V = 10^{-3}$ mm/s) configurations, the iterative plasticity algorithm failed to converge before the loading process was completed. The maximum shear strain reached at the cylinder wall when algorithm failure occurs is $\varepsilon_d \approx 2\%$ for the partially drained condition, and is $\varepsilon_d \approx 4.5\%$ for the fully drained condition. These numerical difficulties are mainly attributed to the very low value of the material cohesion ($c = 2$ kPa). As a matter of fact, the F.E calculations converged in all cases when the value of material cohesion was increased by ten times. In the context of Drucker-Prager like models, it has been long recognized that convergence difficulties, related to non-associated plastic flow and singularity

Proceedings of the XXXVIII Iberian Latin-American Congress on Computational Methods in Engineering
P.O. Faria, R.H. Lopez, L.F.F. Miguel, W.J.S. Gomes, M. Noronha (Editores), ABMEC, Florianópolis, SC, Brazil, November 5-8, 2017.

of cone peak (apex), appear in typical return-mapping schemes when the computed trial stresses fall within tensile regions outside the yield surface (one may refer for instance to Hjiaj et al. (2003) or Lambrecht and Miehe (1999) for an indepth discussion on the issue).

Referring to the results shown in Figures 5(a) and 5(b), it is observed that the maximum shear stress mobilized at cylinder wall turns to be very sensitive to the rotation rate. Both the non-linear poroelastic model and poroplastic F.E solutions predict decreasing values for the maximum shear stress as the rotation rate increases, passing from the fully drained regime to undrained regime. It also appears from these figures that the value of initial zone of influence a_0 slightly affects the magnitude of maximum shear q_u mobilized at the cylinder wall in both cases of rotation rates $V = 1\,\text{mm/s}$ (close to undrained conditions) and $V = 10^{-5}\,\text{mm/s}$ (fully drained regime). In contrast, the value of q_u is more sensitive to the value of a_0 when the loading is applied at intermediate velocity $V = 10^{-3}\,\text{mm/s}$ (partially drained conditions).

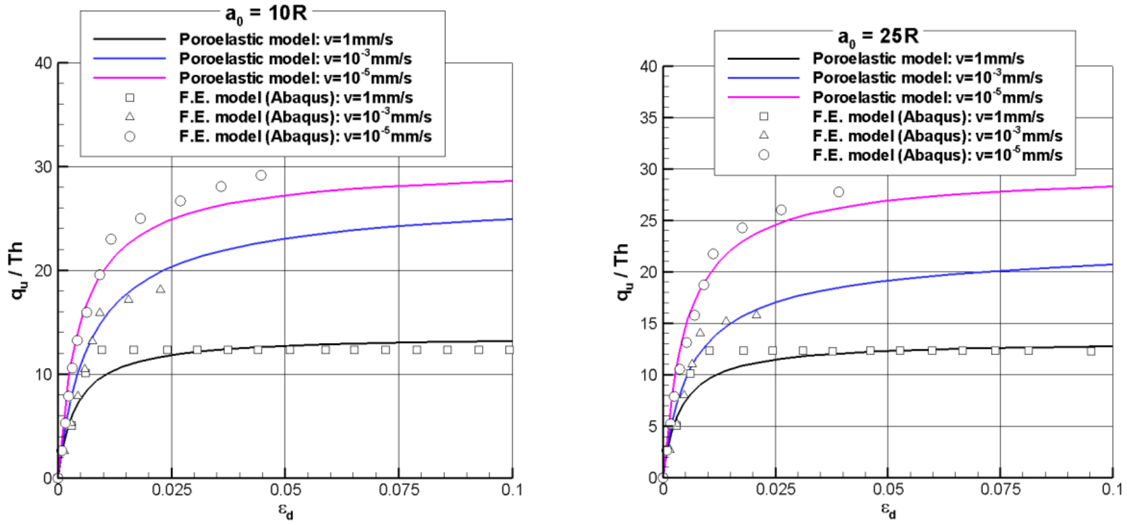

(a) $a_0 = 10R$ (b) $a_0 = 25R$

Figure 5: Normalized shear stress versus equivalent deviatoric strain at the rotating cylinder wall.

Calling that $q_u = \sigma_d(r = R)$ is the shear stress and denoting by $p' = -\sigma'_m(r = R)$ the mean effective stress, the evolution of stress states (q_u, p') of soil elements adjacent to the rotating cylinder is shown in Figure 6. The Cambridge $q_u - p'$ space illustrating the stress paths during rotation has been normalized by the initial mean effective stress p'_0. Regarding the poroplastic F.E simulations, only the results corresponding to converged calculations, namely the situation with $V = 1\,\text{mm/s}$ (undrained evolution), are presented in this figure. A direct comparison between the model predictions and F.E numerical solutions indicates very similar undrained stress paths.

Proceedings of the XXXVIII Iberian Latin-American Congress on Computational Methods in Engineering
P.O. Faria, R.H. Lopez, L.F.F. Miguel, W.J.S. Gomes, M. Noronha (Editores), ABMEC, Florianópolis, SC, Brazil, November 5-8, 2017.

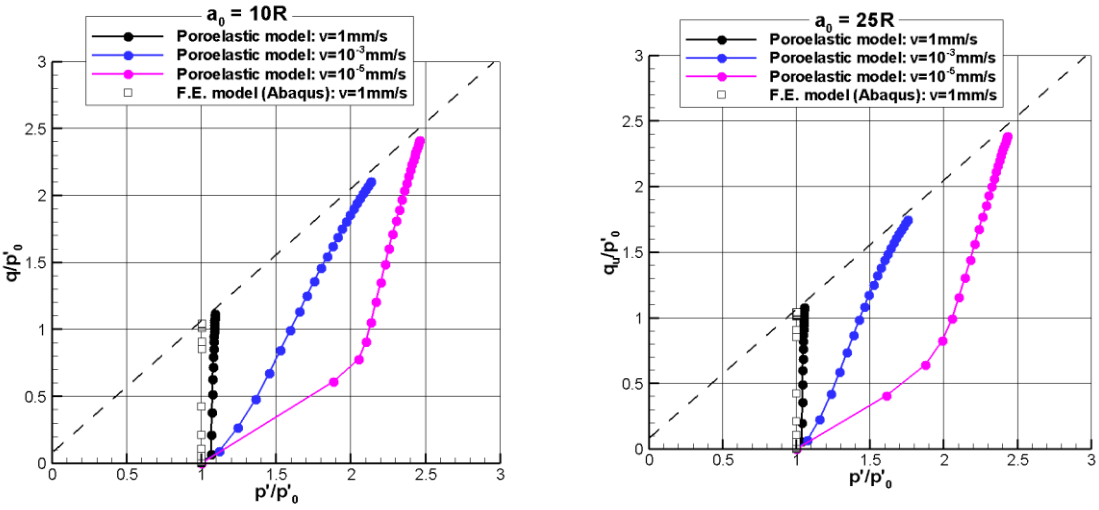

(a) $a_0 = 10R$ (b) $a_0 = 25R$

Figure 6: Numerical and model predictions of stress paths at the rotating cylinder wall.

Figures 7 and 8 respectively display the pore-fluid pressure and shear stress distributions along the soil surrounding the rotating cylinder at the end of loading process. Once again, only the F.E solutions obtained in the converged calculations (undrained condition) shall be presented in the subsequent comparison. In the undrained regime, the comparison with F.E predictions shows that the model is able to capture the main features of soil response regarding both pore pressure and stress distributions. However, the model solutions are reflecting in that situation a slightly faster pore-fluid dissipation in the region close to the rotating cylinder.

The logarithmic-like normalized profiles observed from both model and F.E predictions emphasize once again the significant effects of rotation rate on pore pressure distribution within and beyond the zone of influence $R \le r \le a_0$. The spatial distrinbution is very sensitive to the value of a_0 defining the extent of zone with non-null initial pore pressure distribution. Figure 8 indicates that the distribution of normalized shear stress is also sensitive to the rotation rates, particularly at cylinder wall.

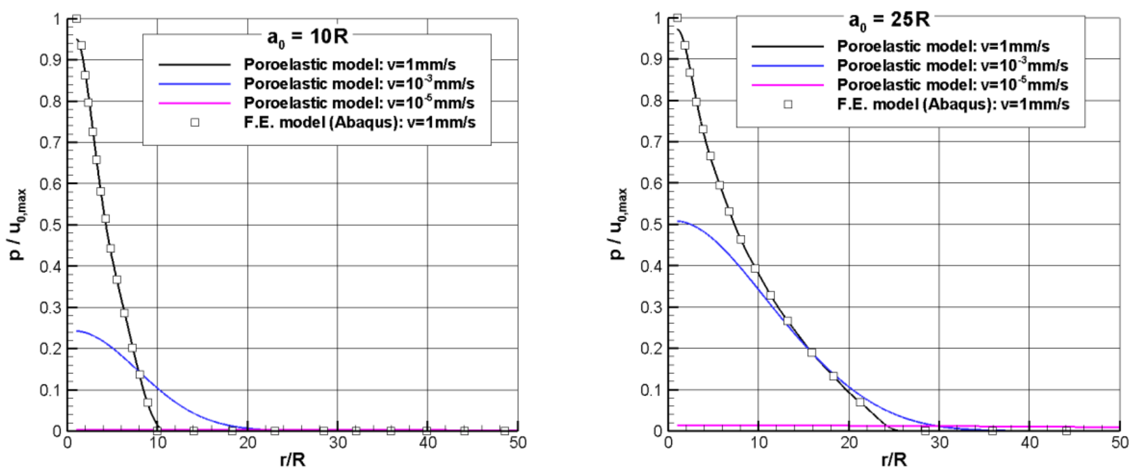

(a) $a_0 = 10R$ (b) $a_0 = 25R$

Figure 7: Distribution of pore-pressure versus radial distance for different rotation rates.

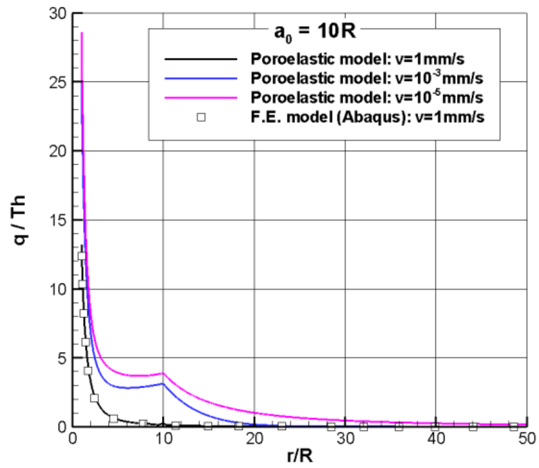

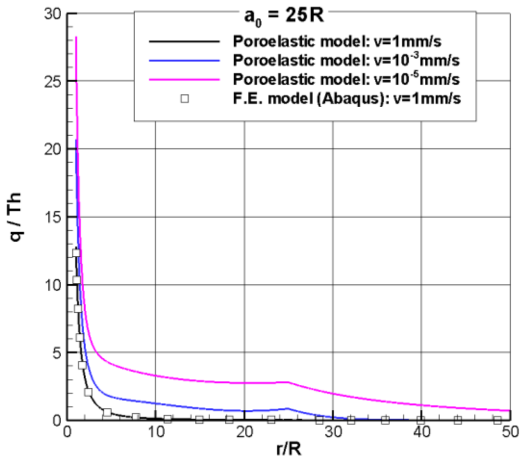

(a) $a_0 = 10R$ (b) $a_0 = 25R$

Figure 8: Distribution of shear stress in the porous medium surrounding the rotating cylinder for different rotation rates.

The effects of drainage conditions in silty porous media can be assessed by plotting the degree of drainage $U^* = 1 - \dfrac{u}{u_{0,\max}}$ versus normalized velocity $V^* = \dfrac{V\,d}{c_h}$. In this case the horizontal consolidation coefficient c_h is evaluated herein from the value of equivalent fluid diffusivity coefficient c_f computed for initial soil shear modulus $G_0 = G(\varepsilon_d = 0, \varepsilon_v = 0)$. Figure 9 displays the model predictions in the space of normalized pore fluid pressure U^* versus normalized velocity V^* for the two extensions of influence zone $a_0 = 10R$ and $a_0 = 25R$. The analysis of these curves proves useful for identifying the order of magnitude of rotation rates that characterize the transition between different drainage regimes. Referring to Figure 9, it appears that transition from drained to partially drained response occurs at a normalized velocity of the order of 10^{-4} (resp. 10^{-5}) for $a_0 = 10R$ (resp. $a_0 = 25R$), whereas the onset of undrained response takes place at normalized velocity of the order of 10^{-1} in both cases. In the range of rotation rates lying between the two transition normalized velocities, partial drainage conditions take place during shearing, which can lead to errors in the evaluation of undrained shear strength, as earlier pointed out by Blight (1968), Torstensson (1977), Chandler (1988) and Biscontin and Pestana (2001).

As regards the sensitivity of pore pressure and shear stress distributions to the extent of a_0, Figure 9 is showing in particular a faster drainage around the rotating cylinder for lower value of a_0 / R, which is associated with a lower distance of drainage.

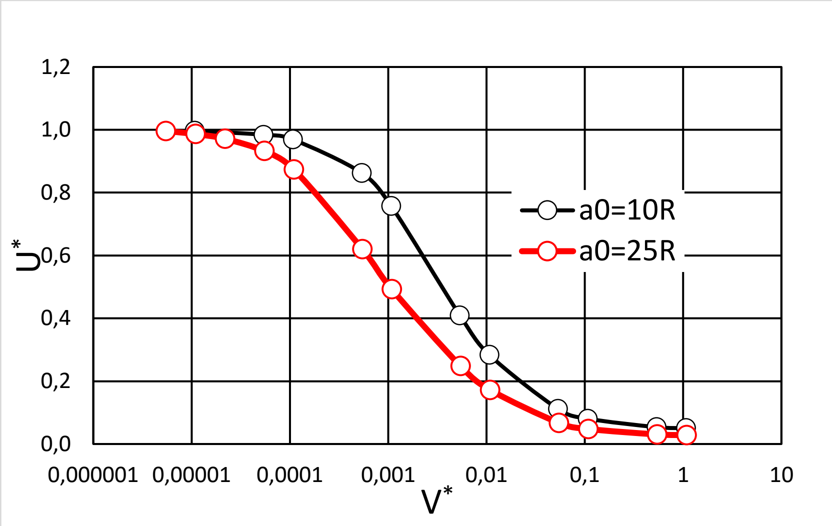

Figure 9: Rate effects on fluid-pore pressure in frictional material: degree of drainage versus normalized velocity.

Associated with the maximum mobilized shear stress, the torque by unit vertical length applied to surrounding soil by the rotating cylinder reads: $C = -2\pi R\, \sigma_{r\theta}(R)$. Sensitivity of this effort to rotation rate can be assessed by plotting in Figure 10 the normalized torque $C^* = C / \sqrt{2}\pi R\, T\, h$ versus normalized velocity V^*. Note that the reference value for applied torque is defined considering $\sigma_{r\theta}(R) = -T\, h / \sqrt{2}$. The figure shows that normalized torque reduces with increasing normalized velocity, producing a drained to undrained torque ratio close to 2.5. As expected, the transition velocities between the different drainage regimes (drained, partially drained, undrained) are similar to those observed for the degree of drainage.

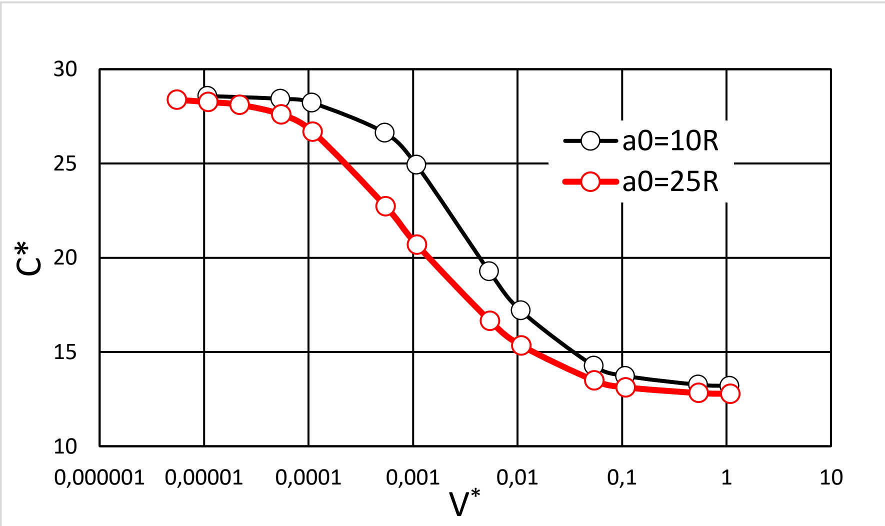

Figure 10: Normalized applied torque versus normalized velocity for frictional material.

4 CONCLUSIONS

Conceived as a simplified approach to flow effects arising in intermediate permeability soils, a non-linear poroelastic model has been formulated to capture the effects of rate rotation on stress and pore-fluid pressure distributions induced in a porous medium surrounding a rigid rotating cylinder. The poromechanical solution to the boundary value problem hence defined amounts to solving a system of two ordinary differential equations governing the components of the skeleton particles displacement. The semi-analytical solutions for pore-fluid pressure, stress and displacement fields are obtained making use of an incremental-iterative algorithm and resorting to a finite difference scheme.

Application of the approach to the case of frictional materials, together with poroplastic F.E simulations, illustrate the ability of the modeling to provide relevant insights into the effects of drainage conditions during cylinder rotation on shear stresses and pore-fluid pressures, as well as their correlation with the soil properties. The results corroborate the fact that partial consolidation in silty soils can affect shear strength measurements from field tests. In particular, the analysis indicated that maximum shear stress mobilized at cylinder wall is very sensitive to rotation rate in frictional materials. Interpretation of the model predictions in terms of normalized velocity V^* versus degree of drainage U^* may help on identifying the transitions from undrained to partially drained response, and from partially drained to fully drained regimes, thus providing useful recommendations for analyzing measured properties.

ACKNOWLEDGEMENTS

The authors gratefully appreciated the financial support provided by the Brazilian Research Council CNPq.

REFERENCES

Abaqus. *ABAQUS User Manual. Dassault Systèmes*, Simulia Corp. ABAQUS© vs. 6.9, Providence, Rohde Island, USA. 2009.

Biot, M.A. (1941). General theory of three-dimensional consolidation. *Journal of Applied Physics*, Vol. 12, pp. 155-164.

Biscontin, G., Pestana, J.M. (2001) Influence of Peripheral Velocity on Vane Shear Strength of an Artificial Clay. *Geotechnical Testing Journal*. ASTM Vol. 24 (4), p. 423-429

Blight, G.E. (1968). A note on field vane testing of silty soils. *Canadian Geotechnical Journal*, Vol. 5, p. 142–149.

de Boer, R. (2000). Theory of Porous Media. Springer-Verlag, Berlin

Chandler, R.J. (1988). The *in situ* measurement of the undrained shear strength of clays using the field vane. In Vane shear strength testing in soils: field and laboratory studies. Edited by A.F. Richards. *American Society for Testing and Materials, Special Technical Publication* 1014, pp. 13–44.

Chung, S. F., Randolph, M. F., Schneider, J. A. (2006). “Effect of penetration rate on penetrometer resistance in clay.” *Journal of Geotechnical and Geoenvironmental Engineering*, 10.1061/(ASCE)1090-0241(2006)132:9(1188), 1188-1196.

Coussy, O., Dormieux, L., Detournay, E. (1998). From mixture theory to Biot's approach for porous media. *International Journal of Solids and Structure*, 35(34-35), 4619-4635.

Coussy, O. (2004). Poro Mechanics. Wiley, UK

DeJong, J.T. Jaeger, R.A, Boulonger, R.W. Randolph, M.F., Wahl, D.A.J. (2012). Variable penetration rate cone testing for characterization of intermediate soils. *Geotechnical and Geophysical Site Characterization 4*.

Dienstmann, G. (2015). *Analysis of in situ test in transient flow*. PhD thesis, Federal University of Rio Grande do Sul, Brazil, (in Portuguese).

Dienstmann, G., Maghous, S., Schnaid, F. (2017). Theoretical analysis and finite element simulation for non-linear poroelastic behavior of cylinder expansion in infinite media under transient pore-fluid flow conditions. *ASCE International Journal of Geomechanics,* 10.1061/(ASCE)GM.1943-5622.0000834.

Dormieux, L., Kondo, D., Ulm, F.-J. (2006). *Microporomechanics*. John Wiley & Sons.

Hjiaj, M., Fortin, J., De Saxé, G. (2003). A complete stress update algorithm for the non-assocoiated Drucker-Prager model including treatment of the apex. *Int. J. Eng. Science*, 41, 1109-1143.

Fayolle, A. (2016). *Non-linear elastic analysis of vane test in a transient flow regime*. Master thesis, Federal University of Rio Grande do Sul, Brazil, (in Portuguese).

House, A.R., Oliveira, J.R.M.S., Randolph, M.F. (2001). Evaluating the coefficient of consolidation using penetration tests. *International Journal of Physical Modelling in Geotechnics*, 1(3): 17-25.

Kim, K., Prezzi, M., Salgado, R., Lee, W. (2008). Effect of penetration rate on cone penetration resistance in saturated clayey soils. *Journal of Geotechnical and Geoenvironmental Engineering*, 10.1061/(ASCE)1090-0241(2008)134:8(1142), 1142-1153.

Lambrecht, M., Miehe, C. (1999). Two non-associated isotropic elastoplastic hardening models for frictional materials. *Acta Mechanica*, 135, 73-90.

Lehane, B.M., O'Loughlin, C.D., Gaudin, C., Randolph, M.F. (2009). Rate effects on penetrometer resistance in kaolin. *Géotechnique*, 59(1), 41–52.

Lemarchand, E., Ulm, F.J., Dormieux, L. (2002). The effect of inclusions on the friction coefficient of highly-filled composite materials. *Journal of Engineering Mechanics*, 10.1061/(ASCE)0733-9399(2002)128:8(876), 876-884.

Maghous, S., Dormieux, L., Barthelemy, J. (2009). Micromechanical approach to the strength properties of frictional geomaterials. *European Journal of Mechanics, A/Solids*, Vol. 28, 179-188.

Maplesoft (2011). *Maple User Manual*, version 15, Waterloo Maple Inc., Toronto.

Morris, P.H., Willians, D.J. (2000). A revision of Blight's model of field vane testing *Canadian Geotechnical Journal*. 37: 1089–1098

Osman, A. S., Randolph, M.F. (2010). Response of a solid infinite cylinder embedded in a poroelastic medium and subjected to a lateral load. *International Journal of Solids and Structures* 47 (2010) 2414–2424

Osman, A.S. (2010). Comparison between Coupled and Uncoupled Consolidation Analysis of a Rigid Sphere in a Porous Elastic Infinite Space. *ASCE Journal of Engineering Mechanics,* 136(8), 1059-1064.

Poulos, H.G., Davis, E.H. (1980). Pile Foundations Analysis and Design, John Wiley and Sons, Inc., USA.

Randolph, M.F., Hope, S.N. (2004). Effect of cone velocity on cone resistance and excess pore pressure. *In: Proceedings of Engineering practice and performance of soft deposits*, Osaka, 147-152.

Randolph, M.F., Wroth, C.P. (1979). An analytical solution for the consolidation around a driven pile. *International Journal for Numerical and Analytical Methods in Geomechanics*, 3(2): 217-229.

Schneider, J.A, Lehane, B.M., Schnaid, F. (2007) Velocity effect of piezocone measurements in normaly and overconsolidation clay. *International Journal of Physical Modelling in Geotechnics*. V 2, p. 23-34

Schnaid, F., Lehane, B. M., Fahey, M. (2004). "In situ test characterization of unusual geomaterials." *Proc., 2nd Int. Conf. on Site Characterization*, Vol. 1, Millpress, Rotterdam, Netherlands, 49–74.

Selvadurai, A.P.S. (2007). The analytical method in geomechanics. *Applied Mechanics Reviews* 60 (3), 87–106.

Silva, M.F. (2005) *Numerical and physical models of rate effects in soil penetration*. PhD thesis, University of Cambridge.

Silva, M.F., White, D.J., Bolton, M.D. (2005). An analytical study of the effect of penetration rate on piezocone tests in clays. *International Journal for Analytical and Numerical Methods in Geomechanics*. pp 501-257.

Torstensson, B. A. (1977). The pore pressure probe. Norsk Jord-Og Fjellteknisk Forbund. Oslo, Foredrag 34.1-34.15. Troedheim, Norway

VÉSIC, A.S. (1972). "Expansion of cavities in infinite soil mass,"Journal of the Soil Mechanics and Foundations Division (JSMFD), *Proceedings of the American Society of Civil Engineers* (ASCE), Vol. 98, No. SM2, pp. 265-290.

Wang, H. (2000). Theory of Linear Poroelasticity with Applications to Geomechanics. Princeton University Press.